Enhanced Osteogenesis of Abalone Shell–Derived Hydroxyapatite via Strontium Substitution and Hyaluronic Acid Incorporation in MC3T3-E1 Osteoblasts

Abstract

Alveolar ridge resorption after tooth extraction is an inevitable physiologic process and can compromise implant site development; therefore, ridge preservation requires bioactive grafts that support early osteoblast colonization and osteogenic signaling. This study evaluated an abalone shell–derived bone graft formulated as carbonated hydroxyapatite (ABG), modified by Sr^{2+} substitution (ABGSr) and supplemented with hyaluronic acid at two ratios (1:1 and 3:4, w/w) to enhance material characteristics, biocompatibility, and osteogenic-related gene expression in MC3T3-E1 osteoblasts. Material characterization included FTIR, SEM, and EDX. FTIR confirmed apatite functional groups (phosphate ~1046 cm^{-1}, hydroxyl ~3572 cm^{-1}, and carbonate bands), supporting successful carbonated hydroxyapatite formation, while SEM showed ABGSr surfaces became rougher and less dense than ABG, suggesting a more cell-favorable topography.

Biocompatibility was assessed by CCK-8 at 24–72 h and compared with a commercial xenograft control (KX) and negative control. ABGSrHA3 (3:4) produced significantly higher optical density than the control at 24, 48, and 72 h, indicating superior proliferation, whereas ABGSrHA1 (1:1) did not exceed the control at 48–72 h. RT-PCR demonstrated significant group-, time-, and interaction-effects for BMP-2, OPN, and OCN. BMP-2 expression peaked early (day 5) with the highest levels in ABGSrHA3, OPN peaked at day 3 with the highest expression in KX, and OCN peaked at day 7 with the highest expression in ABGSrHA1. Overall, Sr^{2+} substitution combined with HA supplementation—particularly the 3:4 formulation—most consistently enhanced early osteoblast proliferation and osteogenic signaling, supporting its potential as a locally sourced ridge preservation biomaterial.

DOI

10.23805/JO.2026.788

Authors

Yosaphat Bayu Rosanto[1]
Intan Ruspita[1]
Cortino Sukotjo[2]
Widowati Siswomihardjo[1*]

1
Universitas Gadjah Mada

2
University of Pittsburgh

* Corresponding Author

Keywords

alveolar ridge resorption, ridge preservation, abalone shell, hydroxyapatite, hyaluronic acid, strontium, FTIR, SEM, EDX, osteoblast proliferation.

INTRODUCTION

Alveolar ridge resorption after tooth extraction is a physiological process that inevitably occurs and cannot be avoided, potentially leading to the need for subsequent ridge augmentation before implant therapy (1). Dimensional loss is most pronounced during early healing; within 12 months, approximately 50% of ridge width can be lost (2), and some reports indicate 50–60% loss may occur within the first three months with gradual continuation thereafter (3). Resorption tends to be greater in the transverse than vertical dimension, especially at the labial/buccal aspect (3,4), contributing to a narrower and shorter ridge architecture. Additionally, experimental evidence describes two concurrent resorptive phases—bundle bone resorption and external surface resorption—leading to clinically relevant vertical and horizontal reductions, particularly at the buccal wall (5).

Socket healing itself is a structured sequence comprising overlapping inflammatory, proliferative, and modeling/remodeling phases (5–7). Early post-extraction dimensional changes are associated with disuse atrophy during the first 7–14 days (3), and modeling is reported to occur earlier than remodeling, with substantial modeling taking place in the first three months (7). Given that resorption is unavoidable, ridge preservation aims to modulate healing to minimize ridge reduction and support bone formation within the extraction socket.

The effectiveness of ridge preservation depends on bone graft materials that act as fillers and scaffolds and support osteoconduction while enabling biological events that culminate in new bone formation (8). In osteoinductive contexts, bone morphogenetic proteins—particularly BMP-2—are widely discussed as key mediators that promote migration, proliferation, and differentiation of osteoprogenitor cells and extracellular matrix production (9,10).

Abalone shell (*Haliotis asinina*) has been explored as a locally sourced calcium precursor for producing carbonated hydroxyapatite (CHA) bone graft materials (11). Its high calcium carbonate content (reported 90–95%) and conversion to calcium oxide provide a strong basis for CHA synthesis (11,12), while carbonate incorporation indicates CHA formation and closer resemblance to the mineral phase of natural bone (13,14). However, highly crystalline grafts may limit osteoclastic resorption and disturb remodeling (15) motivating strategies to reduce crystallinity and improve bioactivity.

Ionic substitution is a recognized approach to tailor hydroxyapatite properties; incorporation of ions such as Sr^{2+} can alter lattice parameters and reduce crystallinity (16–18). In this work, Sr substitution is discussed as lowering lattice order and increasing controlled solubility, facilitating ion release and chemical interactions with the cellular environment (19) SEM observations further indicate that Sr-substituted abalone grafts exhibit rougher surfaces and altered particle spacing, potentially benefiting osteoblast activity and bioactivity.

Beyond inorganic modification, hyaluronic acid has been increasingly applied in oral and maxillofacial contexts (20) and is a key extracellular matrix component in musculoskeletal and dermal tissues (21). In vitro evidence suggests hyaluronic acid can enhance osteoblast formation through improved mesenchymal cell differentiation and migration (22). The dissertation further frames hyaluronic acid as a "conditioning film" that increases hydrophilicity and facilitates early osteoblast adhesion (23), while Sr substitution may promote osteoblast differentiation through reduced crystallinity (24).

Therefore, this study aimed to enhance material characterization, biocompatibility, and osteogenic properties of abalone shell–derived bone grafts through Sr substitution and hyaluronic acid supplementation, evaluated in vitro using MC3T3-E1 cells and the expression of BMP-2, osteopontin (OPN), and osteocalcin (OCN).

MATERIALS AND METHODS

Preparation of Abalone Shell–Derived Bone Graft

Abalone shells (*Haliotis asinina*) were cleaned, dried, and processed to obtain calcium carbonate powder. The powder was thermally treated to produce calcium oxide, followed by wet chemical precipitation to synthesize carbonated hydroxyapatite, hereafter referred to as abalone bone graft (ABG). Strontium-substituted hydroxyapatite (ABGSr) was prepared by partially replacing calcium ions with strontium ions during the precipitation process. The resulting precipitates were filtered, washed, dried, and sintered under controlled conditions to obtain stable graft powders (Figure 1).

To improve biological performance, hyaluronic acid was incorporated into ABGSr at two different weight ratios. The first formulation contained ABGSr and hyaluronic acid at a 1:1 ratio (ABGSrHA1), while the second formulation used a 3:4 ratio (ABGSrHA3). All materials were sterilized prior to biological testing. A commercially available xenograft (KX) was used as a positive control, while cells cultured without graft material served as the negative control.

Material Characterization

Functional group analysis was performed using Fourier-transform infrared spectroscopy (FTIR) to confirm the formation of hydroxyapatite and carbonate substitution. Spectra were recorded in the range of 400–4000 cm^{-1}. Surface morphology and particle characteristics were examined using scanning

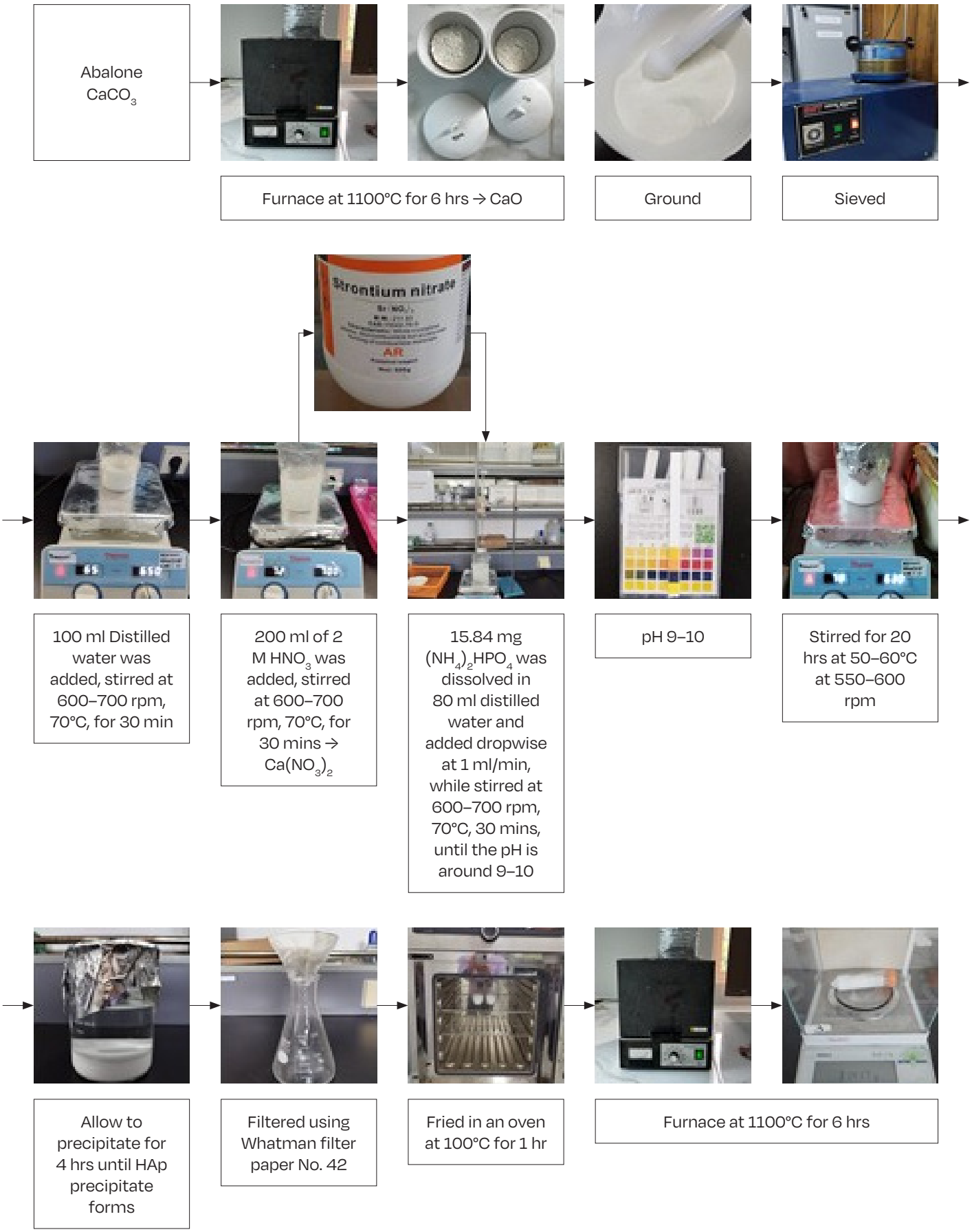

Fig. 1 Material preparation.

electron microscopy (SEM). Elemental composition and ion distribution, including calcium, phosphorus, and strontium, were analyzed using energy-dispersive X-ray spectroscopy (EDX).

Cell Culture

MC3T3-E1 mouse pre-osteoblast cells were used for in vitro evaluation. Cells were cultured in α-minimum essential medium supplemented with fetal bovine serum and antibiotics, and maintained under standard conditions (37 °C, 5% CO_2). Cells were subcultured upon reaching appropriate confluency and used between predetermined passage numbers to ensure consistency.

Cell Proliferation and Viability Assay

Cell proliferation and viability was assessed using the Cell Counting Kit-8 (CCK-8) assay. Cells were seeded in well plates and allowed to attach prior to exposure to the test materials. ABGSrHA1, ABGSrHA3, control, and KX were added to the respective wells. Cell proliferation and viability was evaluated at 24, 48, and 72 hours by measuring absorbance at 450 nm using a microplate reader. Proliferation and viability results were expressed as optical density values relative to the control.

Osteogenic Gene Expression Analysis

To evaluate osteogenic potential, the expression of bone morphogenetic protein-2 (BMP-2), osteopontin (OPN), and osteocalcin (OCN) was analyzed using real-time polymerase chain reaction (RT-PCR). Cells were cultured with the respective materials and harvested at day-3, 5, 7, 10, and 14. Total RNA was extracted, reverse-transcribed into complementary DNA, and amplified using specific primers for each target gene. Gene expression levels were normalized to a housekeeping gene (GAPDH) and expressed as relative fold changes.

Statistical Analysis

All experiments were performed in triplicate or as specified. Quantitative data were expressed as mean ± standard deviation. Statistical analysis was conducted using analysis of variance (ANOVA), followed by appropriate post hoc tests to determine significant differences between groups.

RESULT

Chemical Composition of Abalone Shell–Derived Bone Graft

Fourier-transform infrared spectroscopy (FTIR) was used to analyze the chemical composition of the abalone shell–derived bone graft, focusing on phosphate, carboxyl, and hydroxyl functional groups as characteristic features of calcium hydroxyapatite. Spectra were recorded in the range of 4000–500

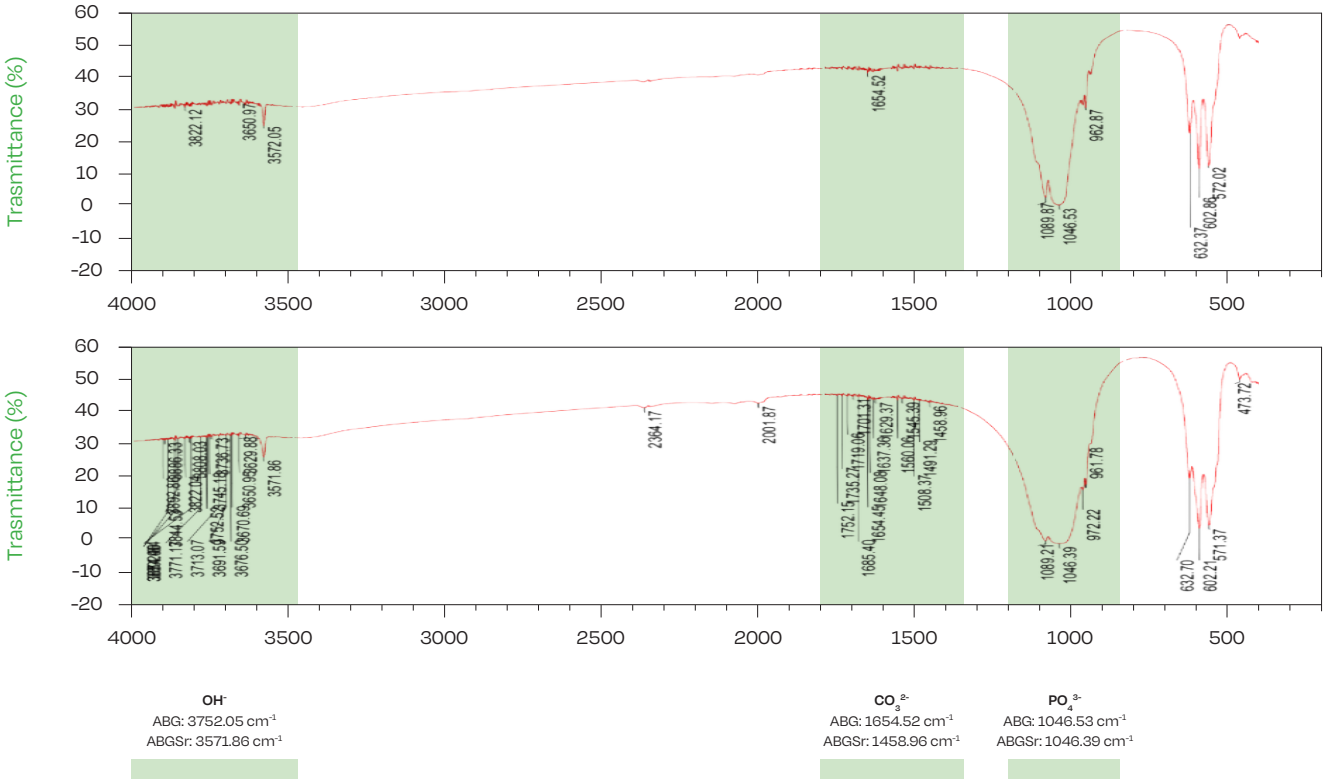

Fig. 2 FTIR spectra demonstrating that both ABG and ABGSr materials consist of calcium hydroxyapatite containing phosphate, carboxyl, and hydroxyl functional groups.

Element	Atom % (ABG)	Atom % (ABGSr)
C	6.86 ± 0.03	8.29 ± 0.03
O	47.25 ± 0.12	49.75 ± 0.09
P	17.69 ± 0.05	15.94 ± 0.04
Ca	28.20 ± 0.09	24.87 ± 0.06
Sr	–	1.15 ± 0.01
Total	100.00	100.00

Tab. 1 Atomic percentage of hydroxyapatite elements in ABG and ABGSr determined by SEM–EDX.

cm^{-1}. The results showed that phosphate groups were observed at 1046.53 cm^{-1} in the ABG group and 1046.39 cm^{-1} in the ABGSr group. Carboxyl groups were detected at 1654.52 cm^{-1} in ABG and 1458.96 cm^{-1} in ABGSr, while hydroxyl groups appeared at 3572.05 cm^{-1} in ABG and 3571.86 cm^{-1} in ABGSr (Figure 2).

These findings indicate that both ABG and ABGSr fabrication processes resulted in calcium hydroxyapatite containing phosphate, carboxyl, and hydroxyl ionic groups. The presence of carboxyl groups confirms that carbonate incorporation into the hydroxyapatite structure was successfully achieved.

Calcium–Phosphate (Ca/P) Ratio

The elemental composition of the synthesized hydroxyapatite materials was analyzed using energy-dispersive X-ray spectroscopy (EDX). The results revealed the presence of carbon (C), oxygen (O), phosphorus (P), and calcium (Ca) in both ABG and ABGSr groups. In addition, strontium (Sr) was detected exclusively in the ABGSr group (Table 1). Based on these data, the calcium-to-phosphate ratio (Ca/P) was calculated.

The Ca/P ratio of the ABG group was 1.59, while the Ca–Sr/P ratio of the ABGSr group was 1.63. Since the Ca/P ratio of human bone hydroxyapatite typically ranges from 1.62 to 1.83, the ABGSr sample more closely resembles the mineral composition of human bone. The presence of Sr confirms successful substitution of calcium by strontium. The lower intensity of Sr compared to calcium indicates partial substitution, meaning that not all calcium ions were replaced by strontium ions (Table 1).

Surface Morphology

Surface morphology and density of the abalone shell–derived bone graft were examined using scanning electron microscopy (SEM). At 20,000× magnification, the ABG group exhibited relatively uniform grain size with closer interparticle spacing (Figure 3, yellow arrows). The structure indicates that pure ABG tends to have a more controlled particle distribution and consistent morphology compared to ABGSr.

In contrast, ABGSr observed at 1,000× magnification displayed a rougher surface with larger agglomerations than ABG (Figure 2, red arrows). Particle size appeared more heterogeneous, and several larger particles were identified.

Strontium substitution within the hydroxyapatite structure resulted in morphological changes, as evidenced by increased agglomeration and a broader particle size distribution. The ABG group showed smoother surfaces and denser particle packing, whereas ABGSr exhibited more loosely packed particles due to agglomeration (Figure 3). The wider interparticle spacing observed in ABGSr suggests a lower degree of crystallinity, which may be advantageous for medical applications.

Cell Proliferation

Cell Counting Kit-8 (CCK-8) assays were conducted to evaluate cell proliferation and cytotoxicity of ABGSrHA1 and ABGSrHA3 samples. Optical density

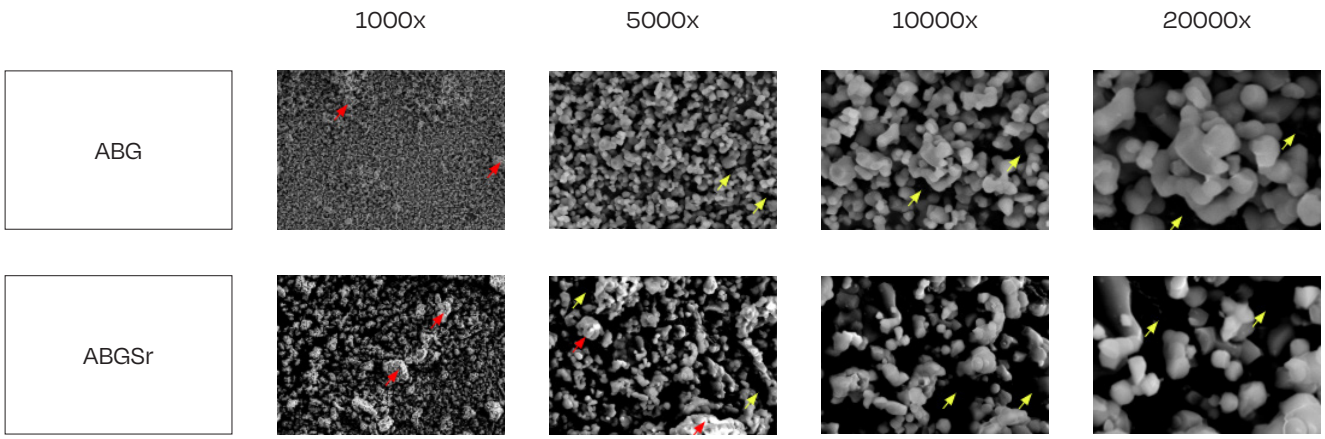

Fig. 3 SEM images showing surface morphology and density of abalone shell–derived hydroxyapatite in ABG and ABGSr groups. Yellow arrows indicate interparticle distance, while red arrows indicate particle agglomeration.

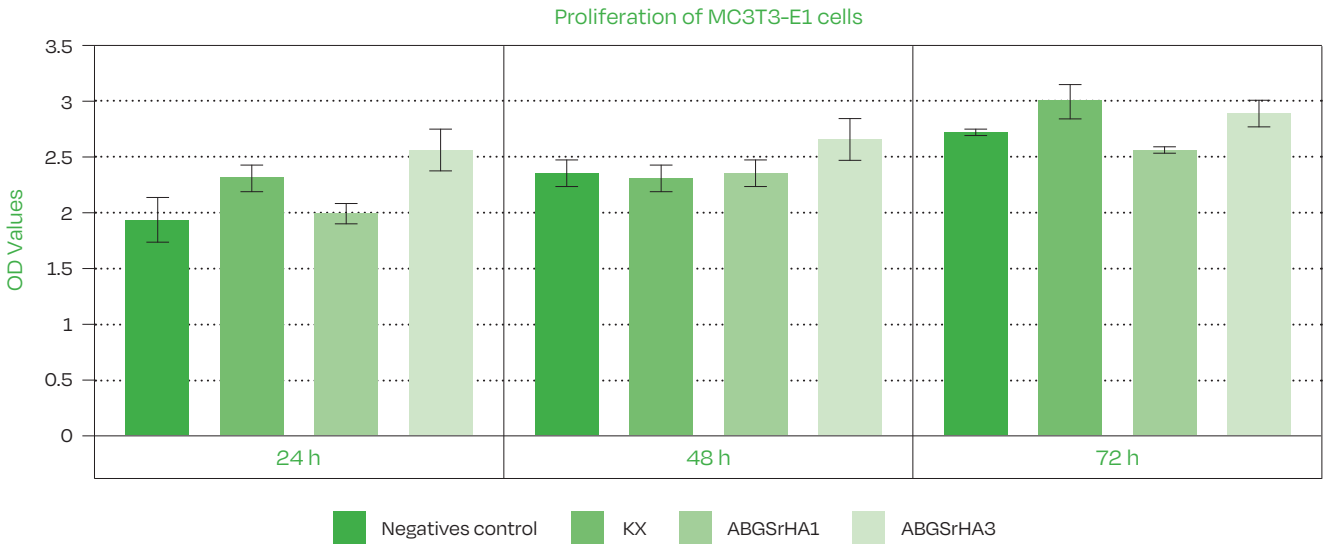

Fig. 4 Mean and standard deviation of MC3T3-E1 cell numbers showing the effects of strontium substitution and hyaluronic acid addition in abalone shell–derived bone grafts on cell proliferation after 24, 48, and 72 hours of culture.

(OD) values in the control group (Figure 4) increased from 1.95, 2.36, and 2.73 over time (24–72 hours), indicating normal cell growth and healthy culture conditions.

The commercial xenograft (KX) showed significantly higher proliferation compared to the control at 24 and 72 hours ($p < 0.05$), with no significant difference at 48 hours ($p > 0.05$). The ABGSrHA1 group did not differ significantly from the control ($p > 0.05$) and tended to show lower values, suggesting that the 1:1 ratio was not optimal for sustaining proliferation. In contrast, ABGSrHA3 demonstrated significantly higher OD values ($p < 0.05$) than the control at 24, 48, and 72 hours, with the strongest significance observed at 24 and 48 hours. These results indicate that strontium substitution combined with hyaluronic acid at a 3:4 ratio was most effective in promoting MC3T3-E1 osteoblast proliferation, particularly during the early phase critical for cell colonization on bone graft materials.

Cell Viability

Cell viability was calculated based on OD values obtained from the CCK-8 assay using the formula in figure 5.

The ABGSrHA1 group showed no significant difference compared to KX at 48 hours but was significantly lower ($p < 0.05$) than KX at 24 and 72 hours (Figure 6). These results indicate that ABGSrHA1 provided inferior cell viability compared to KX, with a transient improvement at 48 hours. The ABGSrHA3 group exhibited significantly higher viability than KX ($p < 0.05$), indicating that strontium substitution combined with hyaluronic acid at a 3:4 ratio most effectively enhanced cell viability and provided the most favorable microenvironment for MC3T3-E1 osteoblasts.

Three-way ANOVA revealed a significant effect of assay type (proliferation vs. viability) on biocompatibility outcomes ($p < 0.001$). Significant interactions were observed between assay type × group, assay type × time, and assay type × group × time ($p < 0.001$). Post hoc LSD analysis demonstrated that the highest proliferation and viability values were achieved in the ABGSrHA3 group, followed by ABGSrHA1. These findings indicate that the addition of hyaluronic acid and strontium substitution enhanced the biocompatibility of abalone shell–derived bone grafts toward MC3T3-E1 cells, particularly in proliferation and viability assays, without inhibiting cell growth. The optimal formulation was identified as ABGSrHA3.

$$\% \text{ Viability} = \frac{\text{OD Treatment - OD Average of Control Medium}}{\text{OD Average of Control Cell - OD Average of Control Medium}} \times 100\%$$

Fig. 5

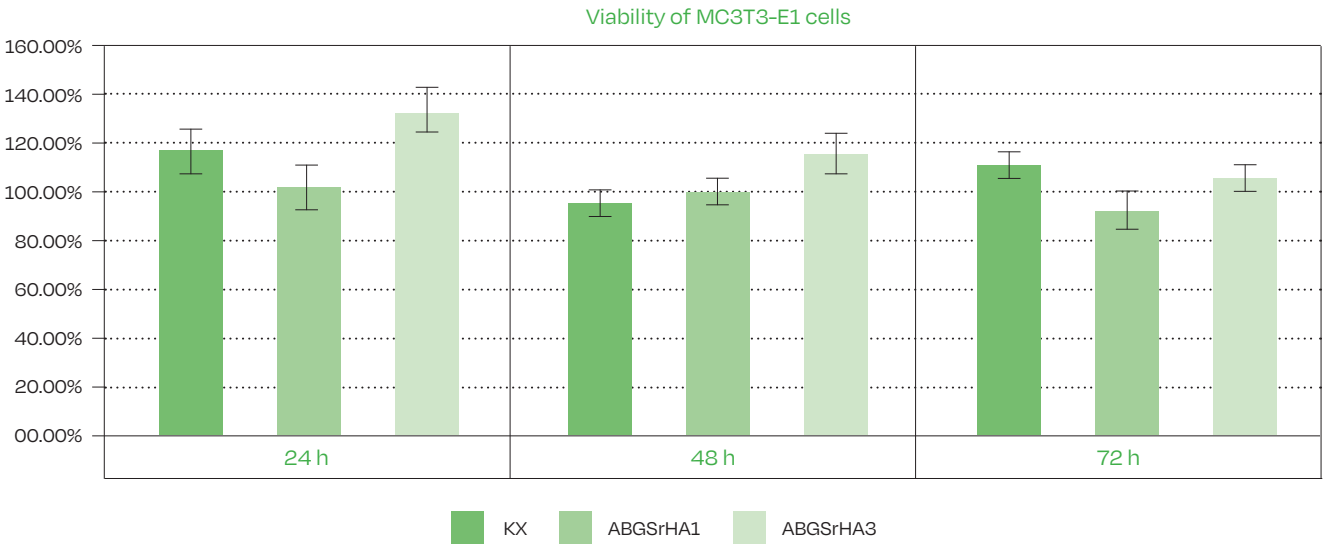

Fig. 6 Mean and standard deviation of MC3T3-E1 cell numbers illustrating the effects of strontium substitution and hyaluronic acid addition in abalone shell–derived bone grafts on cell viability after 24, 48, and 72 hours of culture.

Bone Morphogenetic Protein-2 (BMP-2)

After day 5, BMP-2 expression decreased in all groups (Figure 7), indicating that osteoblasts had progressed toward advanced differentiation and were producing their own extracellular matrix independently of the material stimulus. This finding suggests that strontium substitution and hyaluronic acid addition activated BMP-2 expression in osteoblasts, which was subsequently secreted into the extracellular matrix. After day 7, BMP-2 expression declined in all groups, reflecting the bone tissue maturation phase.

Osteopontin (OPN)

OPN expression peaked on day 3 and decreased thereafter (Figure 8). The highest osteopontin expression was observed in the positive control group,

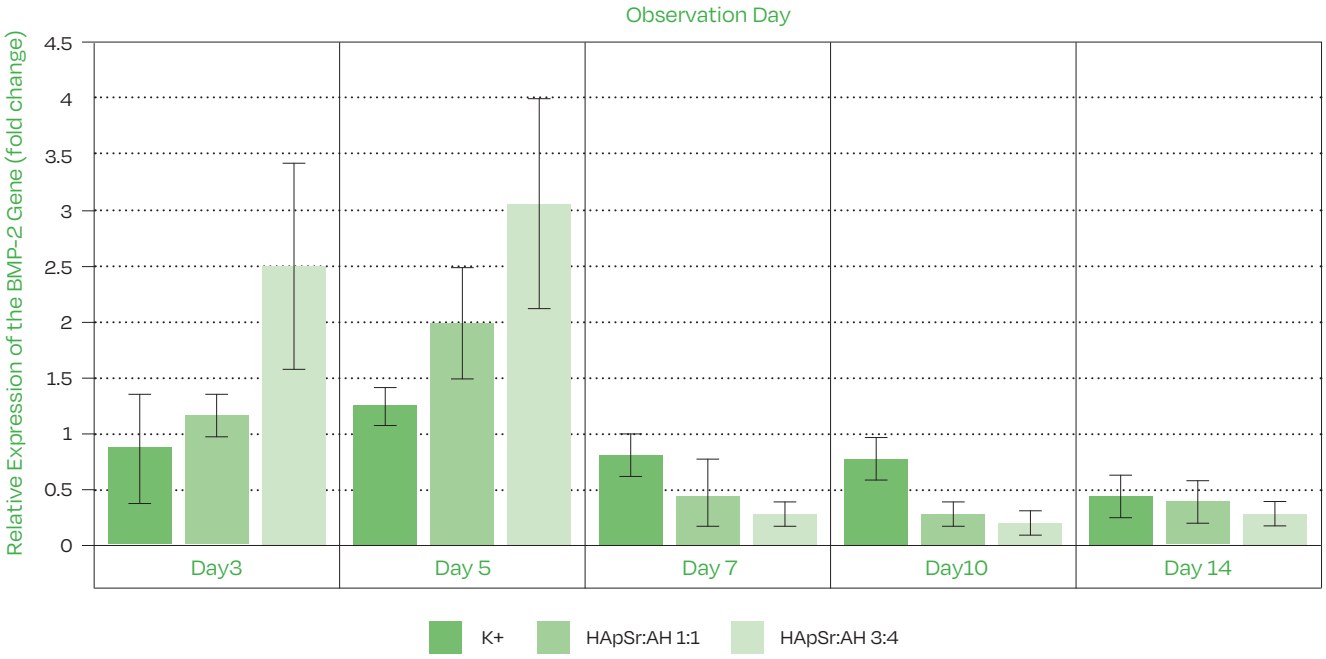

Fig. 7 Demonstrates significant differences in BMP-2 gene expression among bone graft groups and across observation times. Treatment group effects were significant ($p < 0.005$), as were time effects ($p < 0.005$), with a significant group × time interaction ($p = 0.005$). The highest mean BMP-2 expression was observed in the ABGSrHA3 group, particularly on days 3 and 5, reflecting an early cellular response to the material.

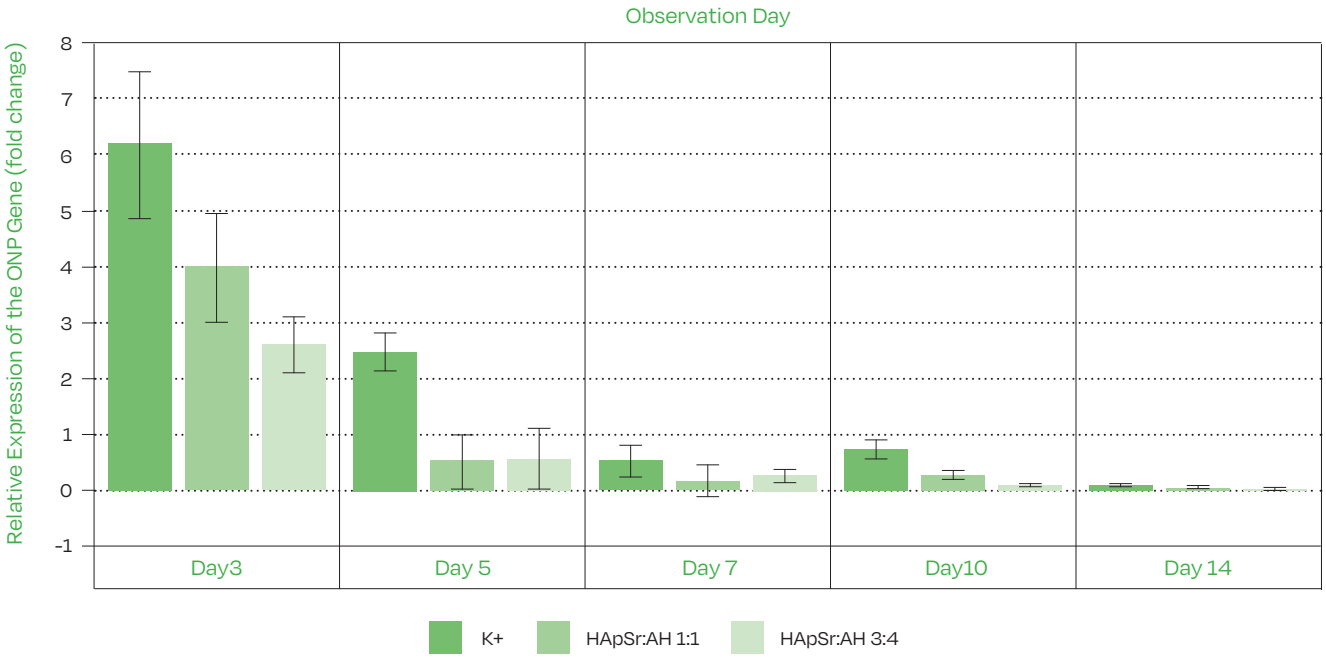

Fig. 8 Shows significant differences in OPN expression among treatment groups ($p < 0.001$) and across observation times ($p < 0.001$), with a significant group × time interaction ($p = 0.002$).

indicating strong osteoblast responsiveness during the early phase. As osteoblast differentiation progressed, the influence of external stimulation diminished. The ABGSrHA1 and ABGSrHA3 groups exhibited a slower and more stable decline, suggesting that these compositions may prolong the differentiation phase and extracellular matrix formation.

Osteocalcin (OCN)

The lowest OCN expression was observed in the ABGSrHA3 group on day 10 (Figure 9), while the highest expression occurred in the ABGSrHA1 group on day 7. Significant differences in OCN gene expression were found among treatment groups ($p = 0.003$) and observation times ($p = 0.001$), with a significant group

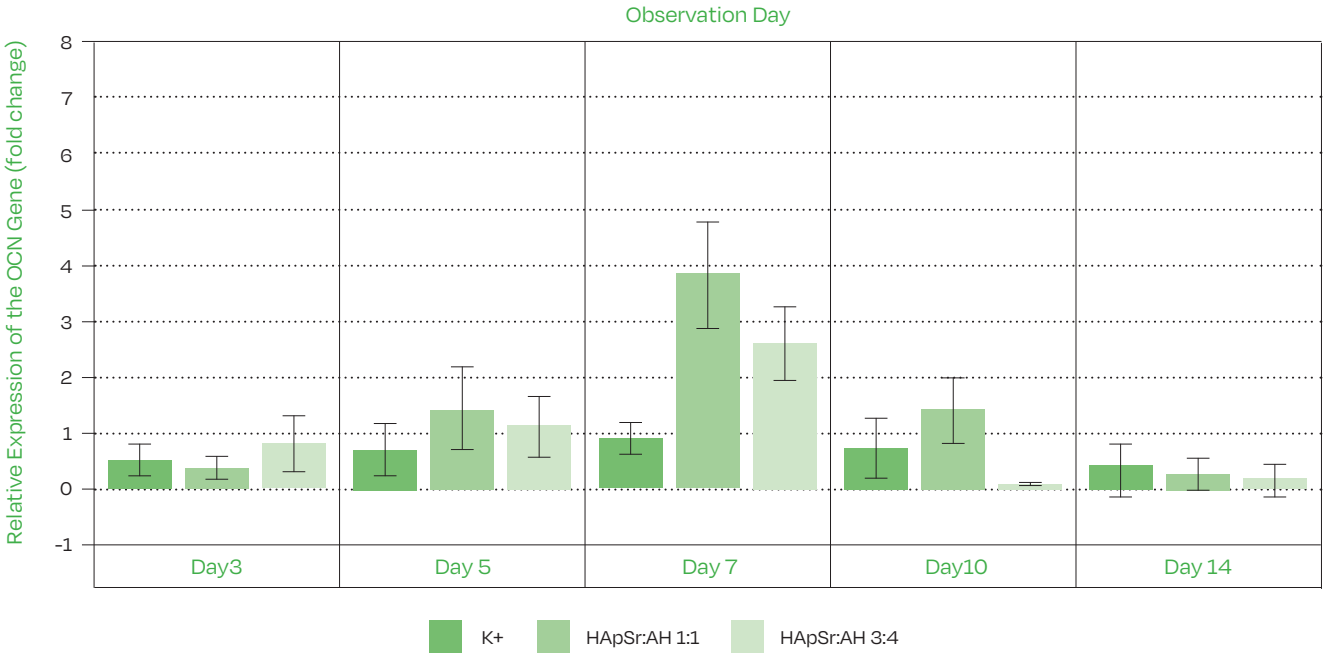

Fig. 9 Mean and standard deviation of MC3T3-E1 cells showing relative expression of the OCN gene.

× time interaction (p = 0.004).

DISCUSSION

This study highlights several important advances in the development of a bioactive bone graft derived from abalone shell through strontium substitution and hyaluronic acid supplementation. The principal novelty lies in the combined physicochemical and biological optimization of a locally sourced xenograft material to more closely resemble the mineral phase and biological behavior of natural bone.

FTIR analysis confirmed that both ABG and ABGSr consist of carbonated hydroxyapatite (CHA), as evidenced by the presence of phosphate, hydroxyl, and carbonate functional groups. The detection of carbonate bands indicates successful carbonation, which is critical because CHA more closely mimics the mineral phase of human bone than stoichiometric hydroxyapatite (13,14). Natural bone mineral is known to be a calcium-deficient, carbonate-rich apatite containing lattice defects, which contribute to higher bioactivity, enhanced protein adsorption, and controlled biodegradability (25,26). Compared with highly crystalline hydroxyapatite, CHA exhibits improved remodeling capacity and osteoblast interaction, supporting its suitability for bone regeneration applications (27,28).

Strontium substitution further refined the mineral chemistry of the graft. The Ca+Sr/P ratio of ABGSr was closer to that of natural bone compared with Ca/P ratio of ABG, and the presence of Sr confirmed partial ionic substitution. Such substitution is known to reduce lattice order and crystallinity, thereby increasing controlled solubility and ion release, which are key drivers of osteogenic signaling (19,29,30). SEM observations corroborated these changes, showing a rougher and less densely packed surface in ABGSr. Surface roughness and microstructural heterogeneity are well recognized to enhance osteoblast adhesion and biological activity, contributing to improved graft–bone interactions.

Functionally, the biological assays demonstrated a synergistic effect between strontium substitution and hyaluronic acid supplementation. The ABGSrHA3 formulation consistently yielded the highest proliferation and viability values, particularly during the early culture period (24–48 h), which is critical for osteoblast colonization of graft surfaces (31). Hyaluronic acid likely acts as a viscoelastic conditioning film that enhances surface hydrophilicity and facilitates early cell adhesion without impeding nutrient diffusion (23). In contrast, the 1:1 formulation appeared insufficient to fully exploit these biofunctional advantages, underscoring the importance of formulation optimization.

At the molecular level, RT-PCR results supported the cellular findings. BMP-2 expression peaked at early time points, particularly in the ABGSrHA3 group, reflecting early osteogenic induction. BMP-2 is a well-established osteoinductive factor that initiates osteoblast differentiation through SMAD-mediated signaling pathways (32–34). The subsequent expression patterns of OPN and OCN followed the expected temporal sequence of osteogenesis, with OPN dominating early matrix interaction phases and OCN marking late-stage maturation (35,36). The relatively higher OCN expression in ABGSrHA1 suggests that different hyaluronic acid concentrations may preferentially modulate distinct stages of osteoblast differentiation.

Importantly, the physicochemical and biological findings obtained in this study were mutually supportive and collectively explain the superior performance of the ABGSrHA3 formulation. Strontium substitution was shown to modify the hydroxyapatite lattice and reduce crystallinity, enabling controlled dissolution of the abalone shell–derived bone graft and sustained release of Ca^{2+} and Sr^{2+} ions. These ions act as key signaling mediators that support osteoblast activity and bone remodeling processes (37). In parallel, the formation of carbonated hydroxyapatite (CHA) combined with a rougher surface topography enhanced serum protein adsorption, thereby exposing adhesion motifs that facilitate faster osteoblast attachment and spreading (38). The addition of hyaluronic acid further amplified these effects; at the 3:4 ratio, hyaluronic acid likely formed a viscoelastic conditioning film that entrapped proteins and stabilized growth factors, while also interacting with RHAMM receptors to strengthen BMP-related signaling and downstream osteogenic pathways (39). Consistent with this mechanism, BMP-2 expression increased at early time points, followed sequentially by OPN expression—associated with integrin/CD44-mediated cell–matrix interactions—and OCN expression as a marker of late osteoblast maturation. Taken together, the coordinated modulation of lattice structure and crystallinity, surface morphology, biocompatibility, and osteogenic gene expression provides a mechanistic basis for why the ABGSrHA3 group consistently outperformed the other formulations evaluated in this study.

Several limitations should be acknowledged. First, this study was conducted entirely in vitro, which cannot fully recapitulate the complex biological and mechanical environment of alveolar bone healing. Second, only two hyaluronic acid ratios were evaluated; a broader range may further refine the optimal formulation. Third, mechanistic pathways were inferred from gene expression patterns rather than confirmed by receptor-blocking or protein-level assays.

Despite these limitations, the findings have important implications for future research and clinical

practice. The ABGSrHA3 formulation demonstrates competitive performance relative to a commercial xenograft during the critical early phase of osteoblast colonization, suggesting potential advantages for ridge preservation after tooth extraction. Its local availability, compositional tunability, and favorable bioactivity profile make it a promising candidate for further in vivo validation. Future studies should focus on animal models to evaluate bone formation, graft degradation, and dimensional stability using histomorphometric and micro-CT analyses, as well as mechanistic studies targeting SMAD, CD44, and RHAMM signaling pathways.

Overall, this study demonstrates that strontium-substituted, hyaluronic acid–enhanced abalone shell–derived CHA can effectively promote osteoblast adhesion, proliferation, and osteogenic gene expression. Among the tested formulations, ABGSrHA3 showed the most balanced and robust biological performance, supporting its potential development as a locally sourced bone graft material for ridge preservation and alveolar reconstruction before dental implant placement.

CONCLUSION

This study demonstrated that abalone shell–derived hydroxyapatite can be effectively optimized through strontium substitution and hyaluronic acid supplementation to improve its physicochemical characteristics and biological performance relevant to ridge preservation. Material characterization confirmed the formation of carbonated hydroxyapatite, while strontium substitution modified lattice structure and surface morphology toward a less crystalline and rougher topography, features associated with improved bioactivity.

In vitro biocompatibility assays showed that the combined modification influenced osteoblast responses in a formulation-dependent manner. Among the tested materials, the ABGSrHA3 (3:4) formulation consistently supported higher early osteoblast proliferation and viability compared with the control and the 1:1 formulation, indicating a more favorable microenvironment for initial cell colonization. Gene expression analysis further revealed that this formulation promoted an osteogenic sequence characterized by early BMP-2 upregulation, followed by OPN and OCN expression, reflecting coordinated progression from osteogenic induction to matrix interaction and maturation.

Importantly, the convergence of material chemistry, surface morphology, cellular responses, and osteogenic gene expression provides support for the observed biological performance. While these findings do not yet confirm clinical efficacy, we conclude that strontium-substituted, hyaluronic acid–enhanced abalone shell–derived hydroxyapatite—particularly the ABGSrHA3 formulation—has potential as a bioactive bone graft candidate.

From a clinical perspective, this material may offer advantages for ridge preservation following tooth extraction by supporting early osteoblast activity and osteogenic signaling, which are critical for maintaining alveolar bone before implant placement. Further in vivo and translational studies are required to validate bone formation, graft remodeling, and dimensional stability before clinical application can be recommended.

Acknowledgments

The authors would like to thank the Indonesian Education Scholarship (BPI), the Center for Higher Education Funding and Assessment (PPAPT), Ministry of Higher Education, Science, and Technology of the Republic of Indonesia, and the Indonesia Endowment Fund for Education (LPDP) for supporting this research.

REFERENCES

1. MacBeth ND, Donos N, Mardas N. Alveolar ridge preservation with guided bone regeneration or socket seal technique. A randomised, single-blind controlled clinical trial. Clin Oral Implants Res. 2022;33(7):681–99.
2. Lin HK, Pan YH, Salamanca E, Lin Y Te, Chang WJ. Prevention of bone resorption by ha/β-tcp + collagen composite after tooth extraction: A case series. Int J Environ Res Public Health. 2019;16(23):1–11.
3. Ucer C, Khan RS. Extraction Socket Augmentation with Autologous Platelet-Rich Fibrin (PRF): The Rationale for Socket Augmentation. Dent J (Basel). 2023;11(8):1–20.
4. Sun Z, Herring SW, Tee BC, Gales J. Alveolar ridge reduction after tooth extraction in adolescents: An animal study. Arch Oral Biol. 2013;58(7):813–25.
5. Araújo MG, Silva CO, Souza AB, Sukekava F. Socket healing with and without immediate implant placement. Vol. 79, Periodontology 2000. Blackwell Munksgaard; 2019. p. 168–77.
6. Pagni G, Pellegrini G, Giannobile W V., Rasperini G. Postextraction alveolar ridge preservation: Biological basis and treatments. Int J Dent. 2012;1(1):1–13.
7. Araujo MG, Silva CO, Misawa M, Sukekava F. Alveolar socket healing: what can we learn? Periodontol 2000. 2015;68(1):122–34.
8. Roberts TT, Rosenbaum AJ. Bone grafts, bone substitutes and orthobiologics the bridge between basic science and clinical advancements in fracture healing. Organogenesis. 2012;8(4):114–24.
9. Oryan A, Alidadi S, Moshiri A, Bigham-Sadegh A. Bone morphogenetic proteins: A powerful osteoinductive compound with non-negligible side effects and limitations. Vol. 40, BioFactors. Blackwell Publishing Inc.; 2014. p. 459–81.
10. Yu YY, Lieu S, Lu C, Miclau T, Marcucio RS, Colnot C. Immunolocalization of BMPs, BMP antagonists, receptors, and effectors during fracture repair. Bone. 2010;46(3):841–51.
11. Sari M, Hening P, Chotimah, Ana ID, Yusuf Y. Porous structure of bioceramics carbonated hydroxyapatite-based honeycomb scaffold for bone tissue engineering. Mater Today Commun. 2021;26:1–11.
12. Sari M, Hening P, Chotimah, Ana ID, Yusuf Y. Bioceramic hydroxyapatite-based scaffold with a porous structure using honeycomb as a natural polymeric Porogen for bone tissue engineering. Biomater Res. 2021;25(2):1–13.
13. Permatasari HA, Sari M, Aminatun, Suciati T, Dahlan K, Yusuf Y. Nano-carbonated hydroxyapatite precipitation from abalone shell (Haliotis asinina) waste as the bioceramics candidate for bone tissue engineering. Nanomaterials and Nanotechnology. 2021;11(1):1–9.
14. Patty DJ, Nugraheni AD, Dewi Ana I, Yusuf Y. Mechanical Characteristics and Bioactivity of Nanocomposite Hydroxyapatite/Collagen Coated Titanium for Bone Tissue Engineering. Bioengineering. 2022;9(12):1–17.
15. Rolvien T, Barbeck M, Wenisch S, Amling M, Krause M. Cellular mechanisms responsible for success and failure of bone substitute materials. Int J Mol Sci. 2018;19(10):2893.
16. Wang H, Lee J-K, Moursi A, Lannutti JJ. Ca/P ratio effects on the degradation of hydroxyapatite in vitro. J Biomed Mater Res A. 2003;67A(2):599–608.
17. Shi Z, Huang X, Cai Y, Tang R, Yang D. Size effect of hydroxyapatite nanoparticles on proliferation and apoptosis of osteoblast-like cells. Acta Biomater. 2009;5(1):338–45.
18. Leeuwenburgh SCG, Ana ID, Jansen JA. Sodium citrate as an effective dispersant for the synthesis of inorganic-organic composites with a nanodispersed mineral phase. Acta Biomater. 2010;6(3):836–44.
19. Fredholm YC, Karpukhina N, Brauer DS, Jones JR, Law R V., Hill RG. Influence of strontium for calcium substitution in bioactive glasses on degradation, ion release and apatite formation. J R Soc Interface. 2012;9(70):880–9.
20. Huang H, Feng J, Wismeijer D, Wu G, Hunziker EB. Hyaluronic acid promotes the osteogenesis of BMP-2 in an absorbable collagen sponge. Polymers (Basel). 2017;9(8):1–13.
21. Tolg C, McCarthy JB, Yazdani A, Turley EA. Hyaluronan and RHAMM in Wound Repair and the 'cancerization' of Stromal Tissues. Biomed Res Int. 2014;2014:1–18.

22. Aslan M, Şimşek G, Dayi E. The effect of hyaluronic acid-supplemented bone graft in bone healing: Experimental study in rabbits. J Biomater Appl. 2006;20(3):209–20.
23. Iaconisi GN, Lunetti P, Gallo N, Cappello AR, Fiermonte G, Dolce V, et al. Hyaluronic Acid: A Powerful Biomolecule with Wide-Ranging Applications—A Comprehensive Review. Int J Mol Sci. 2023;24(12):1–22.
24. Borciani G, Ciapetti G, Vitale-Brovarone C, Baldini N. Strontium Functionalization of Biomaterials for Bone Tissue Engineering Purposes: A Biological Point of View. Materials. 2022;15(5):1–33.
25. Madupalli H, Pavan B, Tecklenburg MMJ. Carbonate substitution in the mineral component of bone: Discriminating the structural changes, simultaneously imposed by carbonate in A and B sites of apatite. J Solid State Chem. 2017;255(1):27–35.
26. Shah FA. Revisiting the physical and chemical nature of the mineral component of bone. Acta Biomater. 2025;196(1):1–16.
27. Resende RFB, Sartoretto SC, Uzeda MJ, Alves ATNN, Calasans-Maia JA, Rossi AM, et al. Randomized controlled clinical trial of nanostructured carbonated hydroxyapatite for alveolar bone repair. Materials. 2019;12(22):1–13.
28. Yu L, Holmgren A, Zhou M, Hedlund J. Highly permeable CHA membranes prepared by fluoride synthesis for efficient CO2/CH4 separation. J Mater Chem A Mater. 2018;6(16):6847–53.
29. Prekajski M, Mirković M, Todorović B, Matković A, Marinović-Cincović M, Luković J, et al. Ouzo effect-New simple nanoemulsion method for synthesis of strontium hydroxyapatite nanospheres. J Eur Ceram Soc. 2016;36(5):1293–1298.
30. Asghar G, Naeem M, Khusro SN, Iftikhar M, Awan MS, Tariq GH, et al. INFLUENCE OF Sm-Cr DOPING ON STRUCTURAL AND MAGNETIC PROPERTIES OF M-TYPE STRONTIUM HEXAFERRITE. Dig J Nanomater Biostruct. 13(4):915–920.
31. Terriza A, Vilches-Pérez JI, González-Caballero JL, de la Orden E, Yubero F, Barranco A, et al. Osteoblasts interaction with PLGA membranes functionalized with titanium film nanolayer by PECVD. In vitro assessment of surface influence on cell adhesion during initial cell to material interaction. Materials. 2014;7(3):1687–1708.
32. Guo Y, Zhang C qiu, Zeng Q cheng, Li R xin, Liu L, Hao Q xin, et al. Mechanical strain promotes osteoblast ECM formation and improves its osteoinductive potential. Biomed Eng Online. 2012;11(80):1–10.
33. Zhang W, Tian Y, He H, Chen R, Ma Y, Guo H, et al. Strontium attenuates rhBMP-2-induced osteogenic differentiation via formation of Sr-rhBMP-2 complex and suppression of Smad-dependent signaling pathway. Acta Biomater. 2016;33(1):290–300.
34. Liu Z, Yu Z, Chang H, Wang Y, Xiang H, Zhang X, et al. Strontium-containing α-calcium sulfate hemihydrate promotes bone repair via the TGF-β/Smad signaling pathway. Mol Med Rep. 2019;20(4):3555–64.
35. Clemente N, Raineri D, Cappellano G, Boggio E, Favero F, Soluri MF, et al. Osteopontin Bridging Innate and Adaptive Immunity in Autoimmune Diseases. J Immunol Res. 2016;2016:1–5.
36. Cho YD, Shin JC, Kim HL, Gerelmaa M, Yoon HI, Ryoo HM, et al. Comparison of the osteogenic potential of titanium- and modified zirconia-based bioceramics. Int J Mol Sci. 2014;15(3):4442–52.
37. Anutrasakda W, Phasuk A, Tangku C. Effect of different CO32-to PO43-molar ratios on the properties, morphology, and Pb(II) removal performance of carbonated hydroxyapatite. J Environ Chem Eng. 2021;9(1):1–9.
38. Stanislavov AS, Sukhodub LF, Sukhodub LB, Kuznetsov VN, Bychkov KL, Kravchenko MI. Structural features of hydroxyapatite and carbonated apatite formed under the influence of ultrasound and microwave radiation and their effect on the bioactivity of the nanomaterials. Ultrason Sonochem. 2018;42(1):84–96.
39. Dovedytis M, Liu ZJ, Bartlett S. Hyaluronic acid and its biomedical applications: A review. Engineered Regeneration. 2020;1(1):102–13.